Electronic Supplementary Information (ESI)

$M_2As_2Q_5$ (M = Ba, Pb; Q = S, Se): A source of infrared nonlinear optical materials with excellent overall performance activated by multiple discrete arsenate anions

Man-Man Chen,‡[a,d] Zuju Ma,‡[b] Bing-Xuan Li,[e] Wen-Bo Wei,[a,d] Xin-Tao Wu,[a,c] Hua Lin,*[a,c] and Qi-Long Zhu*[a,c]

[a]*State Key Laboratory of Structural Chemistry, Fujian Institute of Research on the Structure of Matter, Chinese Academy of Sciences, Fuzhou 350002, China*

[b]*School of Environmental and Materials Engineering, Yantai University, Yantai 264005, China*

[c]*Fujian Science & Technology Innovation Laboratory for Optoelectronic Information of China, Fuzhou 350002, China*

[d]*University of the Chinese Academy of Sciences, Beijing 100049, China*

[e]*Key Laboratory of Optoelectronic Materials Chemistry and Physics, Fujian Institute of Research on the Structure of Matter, Chinese Academy of Sciences, Fuzhou 350002, China*

‡*M.-M.C. and Z.M. contributed equally to this work.*

*E-mail: linhua@fjirsm.ac.cn and qlzhu@fjirsm.ac.cn

Electronic Supplementary Information Index

1. Experimental Section

1.1 Materials and Instruments

1.2 Synthesis

1.3 Second-Harmonic Generation (SHG) Measurements

1.4 Laser Induced Damage Threshold (LIDT) Measurements

2. Computational Details

3. Figures and Tables

Figure S1-1. The characterizations of $Ba_2As_2Se_5$: (a) SEM image and corresponding elemental mapping analysis and (b) EDX results.

Figure S1-2. The characterizations of $Ba_2As_2S_5$: (a) SEM image and corresponding elemental mapping analysis and (b) EDX results.

Figure S1-3. The characterizations of $Pb_2As_2S_5$: (a) SEM image and corresponding elemental mapping analysis and (b) EDX results.

Figure S2. The experimental (black) and simulated (red) powder XRD of (a) $Ba_2As_2Se_5$, (b) $Ba_2As_2S_5$ and (c) $Pb_2As_2S_5$.

Figure S3. The TG and DTA curves of (a) $Ba_2As_2Se_5$, (b) $Ba_2As_2S_5$ and (c) $Pb_2As_2S_5$.

Figure S4. The coordination environment and bond lengths (Å) of crystallographic independent Ba atoms in $Ba_2As_2Se_5$.

Figure S5. The coordination environment and bond lengths (Å) of crystallographic independent Ba atoms in $Ba_2As_2S_5$.

Figure S6. (a–h) the coordination environment and bond lengths (Å) of crystallographic independent Pb atoms in $Pb_2As_2S_5$ and (b) the ICOHP (eV/bond) plotted against Pb–S distance (Å).

Figure S7. Theoretical calculation results of $Ba_2As_2Se_5$: (a) band structure; (b) PDOSs [only the states with major contributions are given and the Fermi level (E_F) is set at 0.0 eV].

Figure S8. Theoretical calculation results of $Ba_2As_2S_5$: (a) band structure; (b) PDOSs

[only the states with major contributions are given and the Fermi level (E_F) is set at 0.0 eV].

Figure S9. Theoretical calculation results of $Pb_2As_2S_5$: (a) band structure; (b) PDOSs [only the states with major contributions are given and the Fermi level (E_F) is set at 0.0 eV].

Figure S10. The first Brillouin zone with high symmetry points of (a) $Ba_2As_2Se_5$, (b) $Ba_2As_2S_5$ and (c) $Pb_2As_2S_5$.

Figure S11. Energy dependences of the real part (ε_1) and imaginary part (ε_2) of (a) $Ba_2As_2Se_5$, (b) $Ba_2As_2S_5$ and (c) $Pb_2As_2S_5$.

Figure S12. The calculated absorption coefficient (α) of (a) $Ba_2As_2Se_5$, (b) $Ba_2As_2S_5$ and (c) $Pb_2As_2S_5$.

Figure S13. The calculated reflectivity (R) of (a) $Ba_2As_2Se_5$, (b) $Ba_2As_2S_5$ and (c) $Pb_2As_2S_5$.

Table S1 The lattice energy (LE) and lattice energy density (LED).

Table S2 The electronic states or arsenate(III) anions with major contributions in the VBs and CBs for $Ba_2As_2Se_5$.

Table S3 The electronic states or arsenate(III) anions with major contributions in the VBs and CBs for $Ba_2As_2S_5$.

Table S4 The electronic states or arsenate(III) anions with major contributions in the VBs and CBs for $Pb_2As_2S_5$.

4. References

1. Experimental Section

1.1 Materials and Instruments

Raw materials, including Ba (99.9%, Alfa Aesar), As (99.99%, ABCR), S (99.99%, Aladdin), Se (99.999%, Aladdin) and PbS (99.9%, Aladdin) were used as received without further purification. All weighing processes were completed in an anhydrous and oxygen-free glove box. BaS, As_2S_3, BaSe and As_2Se_3 as reactive materials were firstly synthesized for the ternary compounds at a temperature of 1123 K by high-temperature solid-state reaction. The semi-quantitative energy dispersive X-ray (EDX, Oxford INCA) spectra were measured with a field emission scanning electron microscope (FESEM, JSM6700F). Powder X-ray diffraction (PXRD) analysis was carried out in a Rigaku Mini-Flex II powder diffractometer (Cu-K_α, λ = 1.5418 Å). UV-vis-NIR absorption measurement was performed in the region of 200−2500 nm at room temperature using an UV-vis-NIR spectrometer (Perkin-Elmer Lambda 950). The reflectance spectrum of the $BaSO_4$ powder was collected as the baseline and the diffuse reflectance data were converted to absorbance internally by the instrument by use of the Kubelka-Munk function.[1] The thermogravimetric analysis (TGA) was performed on a NETZSCH STA 449C simultaneous analyzer under a constant flow of N_2 atmosphere at a heating rate of 10 K/min.

1.2 Synthesis

Polycrystalline $M_2As_2Q_5$ (M = Ba, Pb; Q = S, Se) were prepared from a mixture of MQ and As_2Q_3 (M = Ba, Pb; Q = S, Se) (molar ratio = 2 : 1) with a total mass of 0.5 g and the mixture was loaded into a dry and clean quartz tube that evacuated to be 10^{-3}

Pa and hydrogen-oxygen flamed-sealed. The tubes were placed in a high-temperature furnace and the temperature was controlled through the computer program that heated to 973 K and keeps them warm for 70 hours, then slowly cooled to 523 K at a rate of 3 K/h. Finally, the temperature controller was turned off, letting them cool to room temperature naturally. The products were taken out from the quartz tubes and observed with a microscope, and it was found that the synthesized crystals were yield-high and stable in air and moisture. The composition M:As:Q of approximately 2 : 2 : 5 was established by EDX with the use of a JSM-6700F SEM. The phase purity of the samples was confirmed by PXRD patterns along with the simulated ones.

1.3 Second-Harmonic Generation (SHG) Measurements

The powder SHG measurements were carried out with the Kurtz-Perry method using a 2050 nm Q-switch laser.[2] $AgGaS_2$ was used as a benchmark material, which is provided by Anhui Institute of Optics and Fine Mechanics, Chinese Academy of Sciences. $M_2As_2Q_5$ (M = Ba, Pb; Q = S, Se) and $AgGaS_2$ were ground and sieved into distinct particle size ranges (30−46, 46−74, 74−106, 106−150, 150−210 μm). The SHG signals of the frequency-doubled output emitted from the sieved samples were detected using a photomultiplier tube and recorded on the oscilloscope.

1.4 Laser Induced Damage Threshold (LIDT) Measurements

The LIDTs of $M_2As_2Q_5$ (M = Ba, Pb; Q = S, Se) at the range of 150−210 μm were measured through single pulse measurement method[3] and crushed $AgGaS_2$ single crystal as the reference. Both samples were packed into identical plastic holders (thickness: 1 mm and diameter: 8 mm). After being exposed to the high-power 1064

nm laser radiation with pulse width τ_p of 10 ns, the apparent change of sample was monitored by an optical microscope. The power of laser beam and the damage spot radius were respectively measured by a Nova II sensor with a PE50-DIF-C energy sensor and a Vernier caliper.

2. Computational Details

The DFT calculations have been performed using the *Vienna ab initio simulation package* (VASP)[4–6] with the Perdew-Burke-Ernzerhof (PBE)[7] exchange correlation functional. The projected augmented wave (PAW)[8] potentials with the valence states 5s, 5p and 6d for Ba, 6s and 6p for Pb, 4s and 4p for As and Se, and 3s and 3p for S, respectively, have been used. A Γ-centered Monkhorst-Pack grid (5×5×5 of $Ba_2As_2Se_5$, 1×3×3 of $Ba_2As_2S_5$, and 3×1×3 of $Pb_2As_2S_5$, respectively) for the Brillouin zone sampling[9] and a cutoff energy of 540 eV for the plane wave expansion were found to get convergent lattice parameters. Both the cell and atomic relaxations were carried out until the residual forces are below 0.02 eV/Å. A Monkhorst-Pack *k*-point mesh (7×7×7 of $Ba_2As_2Se_5$, 5×7×7 of $Ba_2As_2S_5$, and 5×3×5 of $Pb_2As_2S_5$, respectively) was used for the calculation of the linear and nonlinear optical properties.

The imaginary part of the dielectric function due to direct inter-band transitions is given by the expression:

$$\varepsilon_2(\hbar\omega) = \frac{2e^2\pi}{\Omega\varepsilon_0}\sum_{k,v,c}\left|\left\langle\psi_k^c\left|u\cdot r\right|\psi_k^v\right\rangle\right|^2\delta(E_k^c - E_k^v - E) \quad \ldots\ldots\ldots\ldots (1)$$

where Ω, ω, u, v and c are the unit-cell volume, photon frequencies, the vector defining the polarization of the incident electric field, valence and conduction bands,

respectively. The real part of the dielectric function is obtained from ε_2 by a Kramers-Kronig transformation:

$$\varepsilon_1(\omega) = 1 + (\frac{2}{\pi})\int_0^{+\infty} d\omega' \frac{\omega'^2 \varepsilon_2(\omega)}{\omega'^2 - \omega^2} \qquad \text{..... (2)}$$

The refractive index $n(\omega)$ can be obtained based on ε_1 and ε_2.

In calculation of the static $\chi^{(2)}$ coefficients, the so-called length-gauge formalism derived by Aversa and Sipe[10] and modified by Rashkeev et al[11] is adopted, which has proven to be successful in calculating the second order susceptibility for semiconductors and insulators. In the static case, the imaginary part of the static second-order optical susceptibility can be expressed as:

$$\chi^{abc} = \frac{e^3}{\hbar^2\Omega}\sum_{nml,k}\frac{r^a_{nm}(r^b_{ml}r^c_{ln} + r^c_{ml}r^b_{ln})}{2\omega_{nm}\omega_{ml}\omega_{ln}}[\omega_n f_{ml} + \omega_m f_{ln} + \omega_l f_{nm}]$$
$$+ \frac{ie^3}{4\hbar^2\Omega}\sum_{nm,k}\frac{f_{nm}}{\omega^2_{mn}}[r^a_{nm}(r^b_{mn;c} + r^c_{mn;b}) + r^b_{nm}(r^a_{mn;c} + r^c_{mn;a}) + r^c_{nm}(r^a_{mn;b} + r^b_{mn;a})]$$

……(3)

where r is the position operator, $\hbar\omega_{nm} = \hbar\omega_n - \hbar\omega_m$ is the energy difference for the bands m and n, $f_{mn} = f_m - f_n$ is the difference of the Fermi distribution functions, subscripts a, b, and c are Cartesian indices, and $r^b_{mn;a}$ is the so-called generalized derivative of the coordinate operator in k space,

$$r^b_{nm;a} = \frac{r^a_{nm}\Delta^b_{mn} + r^b_{nm}\Delta^a_{mn}}{\omega_{nm}} + \frac{i}{\omega_{nm}} \times \sum_l (\omega_{lm} r^a_{nl} r^b_{lm} - \omega_{nl} r^b_{nl} r^a_{lm}) \qquad \text{..... (4)}$$

where $\Delta^a_{nm} = (p^a_{nn} - p^a_{mm}) / m$ is the difference between the electronic velocities at the bands n and m.

As the nonlinear optical coefficients is sensitive to the momentum matrix, much

finer k-point grid and large amount of empty bands are required to obtain a convergent $\chi^{(2)}$ coefficient. The $\chi^{(2)}$ coefficients here were calculated from PBE wave functions and a scissor operator has been added to correct the conduction band energy (corrected to the experimental gap), which has proven to be reliable in predicting the second order susceptibility for semiconductors and insulators. Besides, some key optical parameters (e.g., energy dependences of the real part (ε_1) and imaginary part (ε_2), absorption coefficient (α), and reflectivity (R)) for $M_2As_2Q_5$ (M = Ba, Pb; Q = S, Se) are shown in Figures S11–13.

3. Figures and Tables

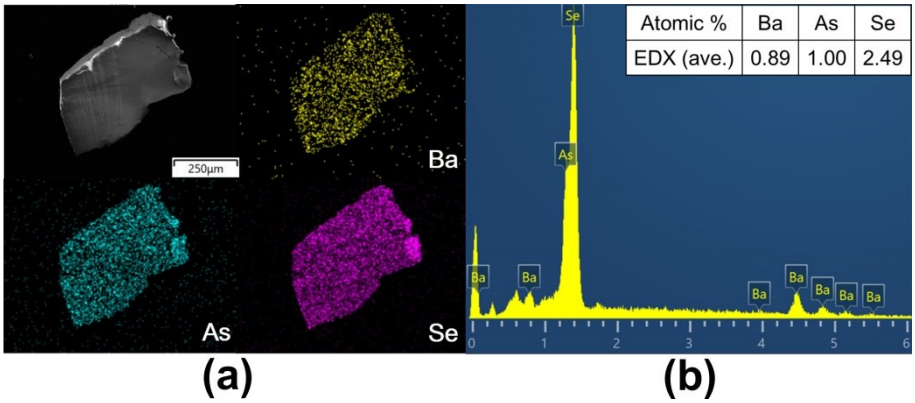

Figure S1-1. The characterizations of $Ba_2As_2Se_5$: (a) SEM image and corresponding elemental mapping analysis and (b) EDX results.

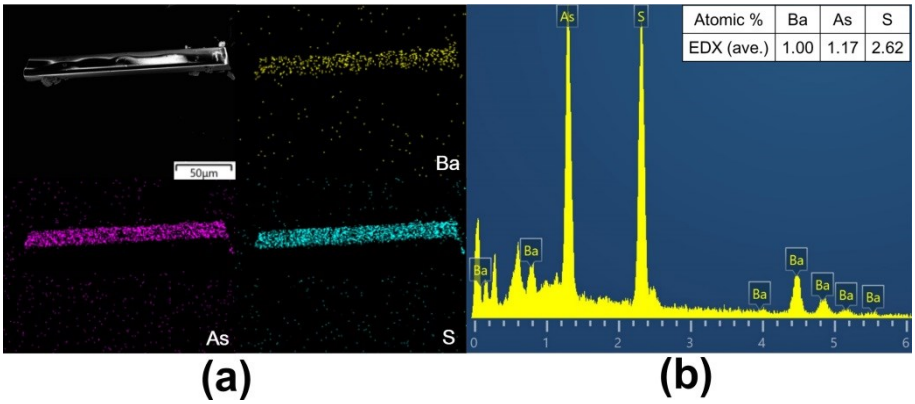

Figure S1-2. The characterizations of $Ba_2As_2S_5$: (a) SEM image and corresponding elemental mapping analysis and (b) EDX results.

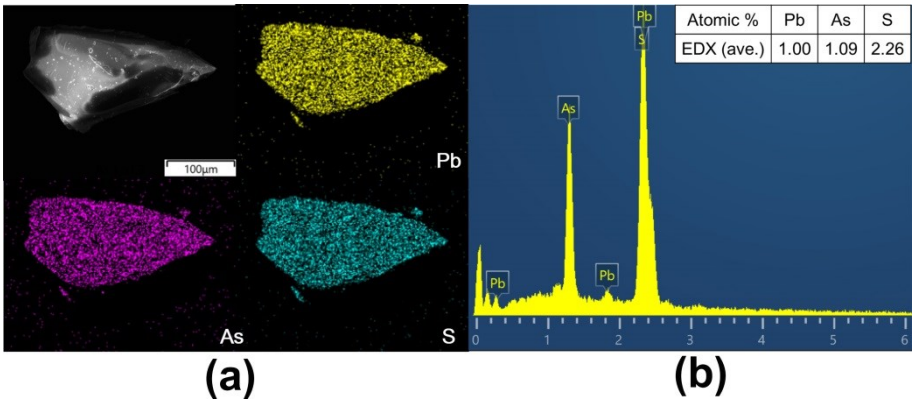

Figure S1-3. The characterizations of $Pb_2As_2S_5$: (a) SEM image and corresponding elemental mapping analysis and (b) EDX results.

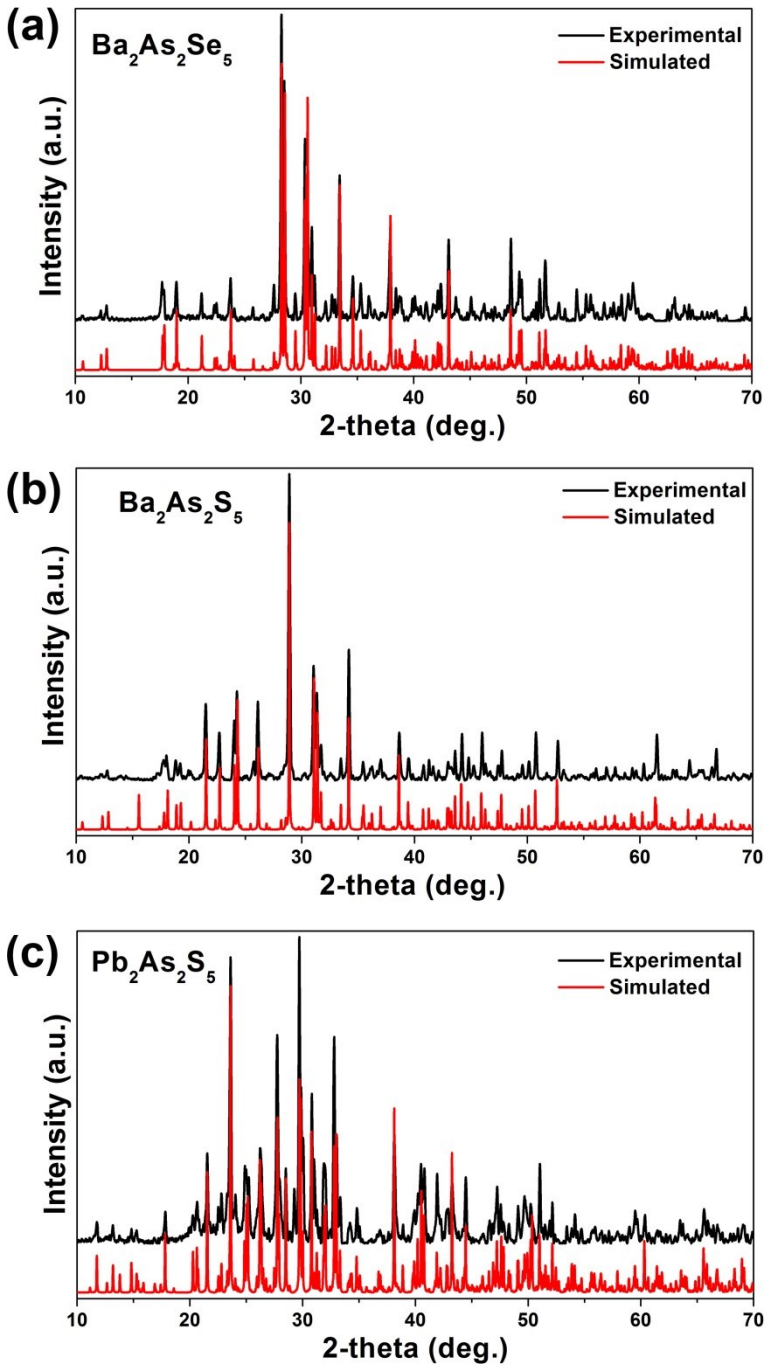

Figure S2. The experimental (black) and simulated (red) PXRD of (a) $Ba_2As_2Se_5$, (b) $Ba_2As_2S_5$ and (c) $Pb_2As_2S_5$.

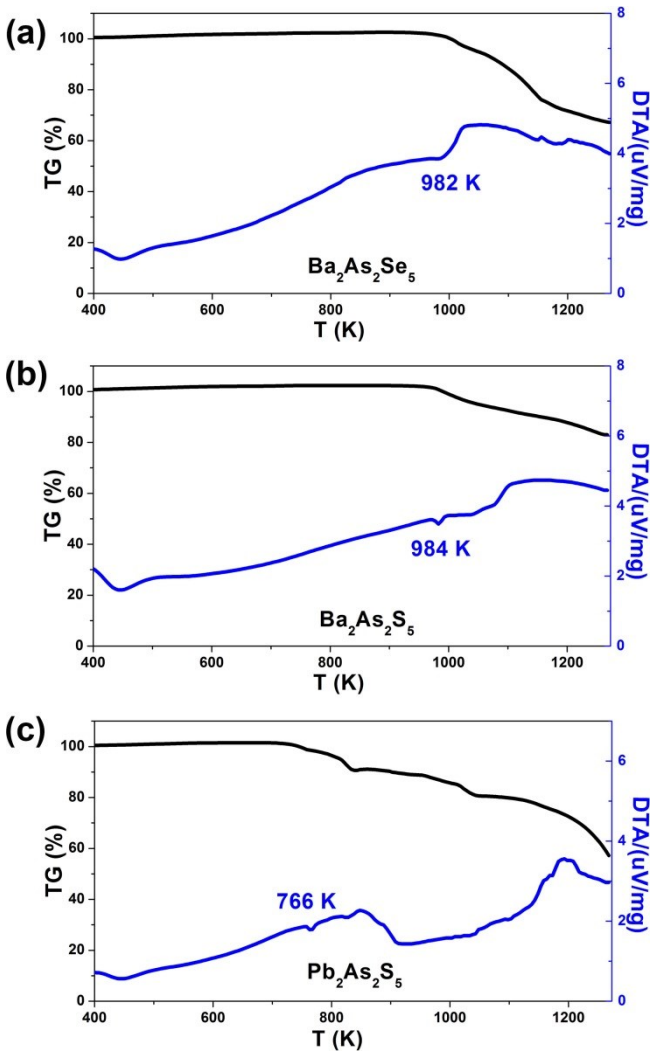

Figure S3. The TG and DTA curves of (a) $Ba_2As_2Se_5$, (b) $Ba_2As_2S_5$ and (c) $Pb_2As_2S_5$.

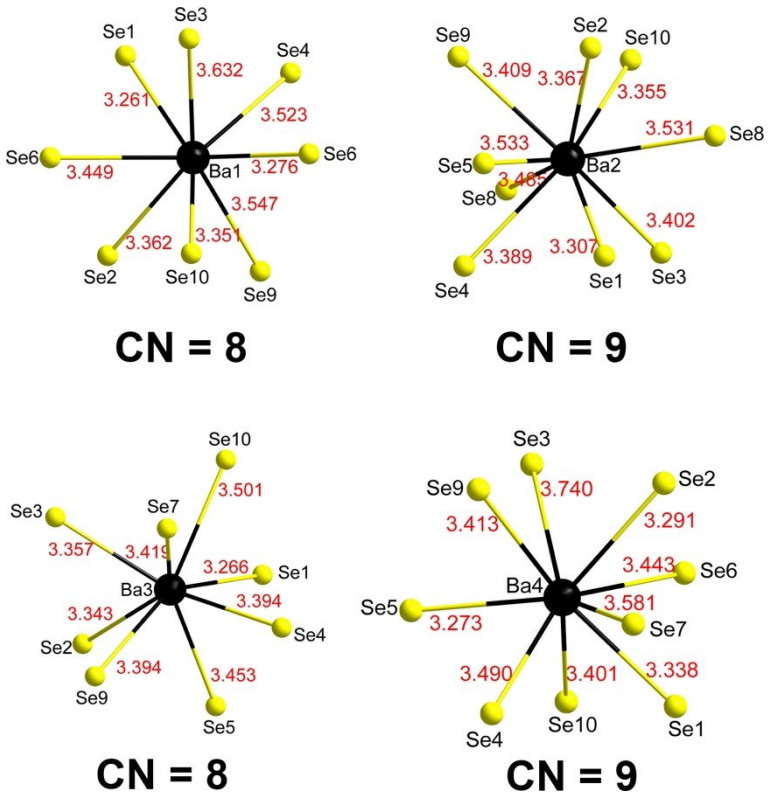

Figure S4. The coordination environment and bond lengths (Å) of crystallographic independent Ba atoms in $Ba_2As_2Se_5$.

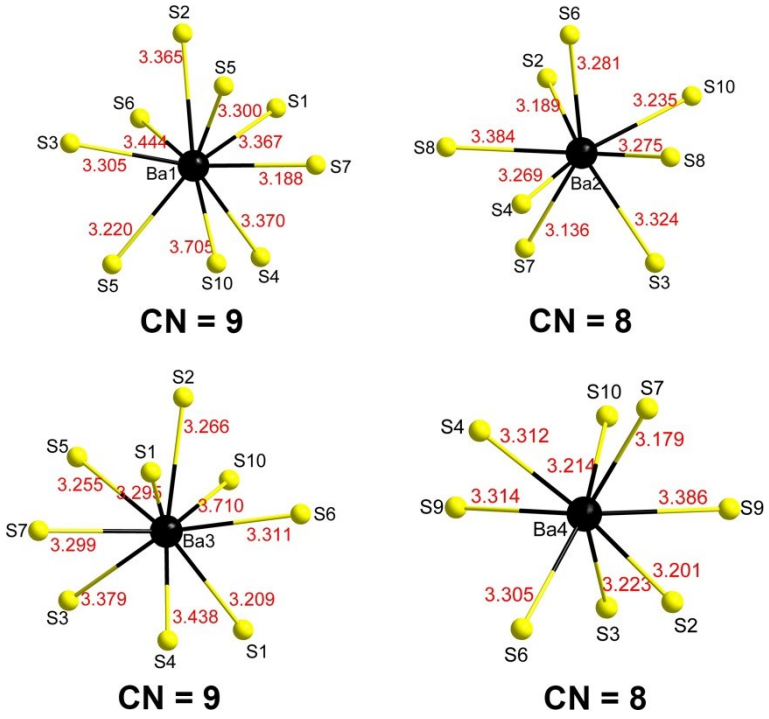

Figure S5. The coordination environment and bond lengths (Å) of crystallographic independent Ba atoms in $Ba_2As_2S_5$.

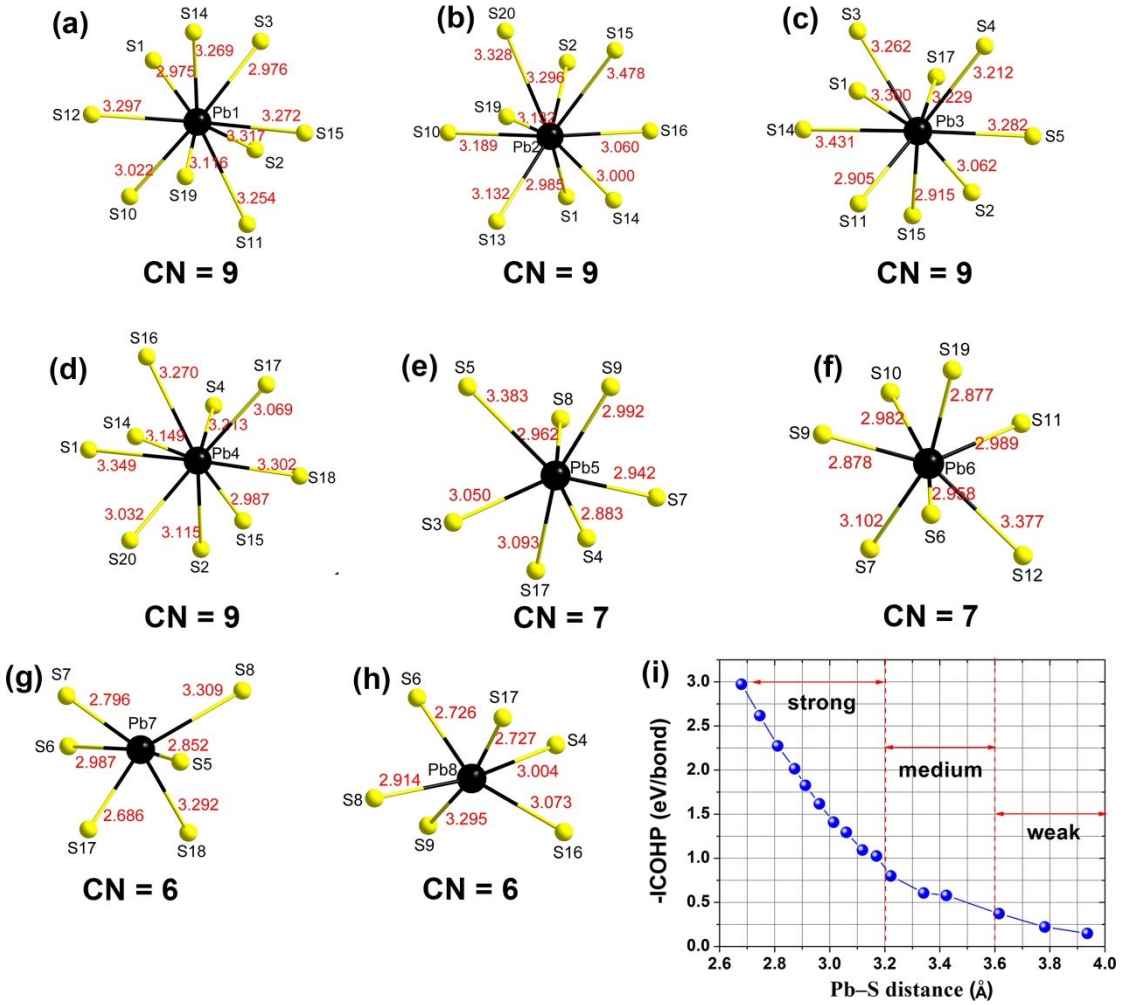

Figure S6. (a–h) The coordination environment and bond lengths (Å) of crystallographic independent Pb atoms in $Pb_2As_2S_5$ and (b) the ICOHP (eV/bond) plotted against Pb–S distance (Å).

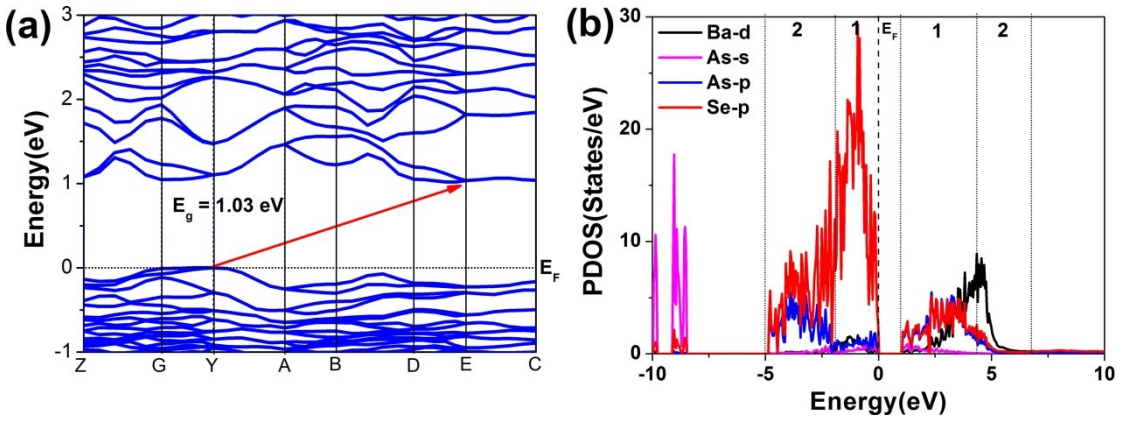

Figure S7. Theoretical calculation results of $Ba_2As_2Se_5$: (a) band structure; (b) PDOSs [only the states with major contributions are given and the Fermi level (E_F) is set at 0.0 eV].

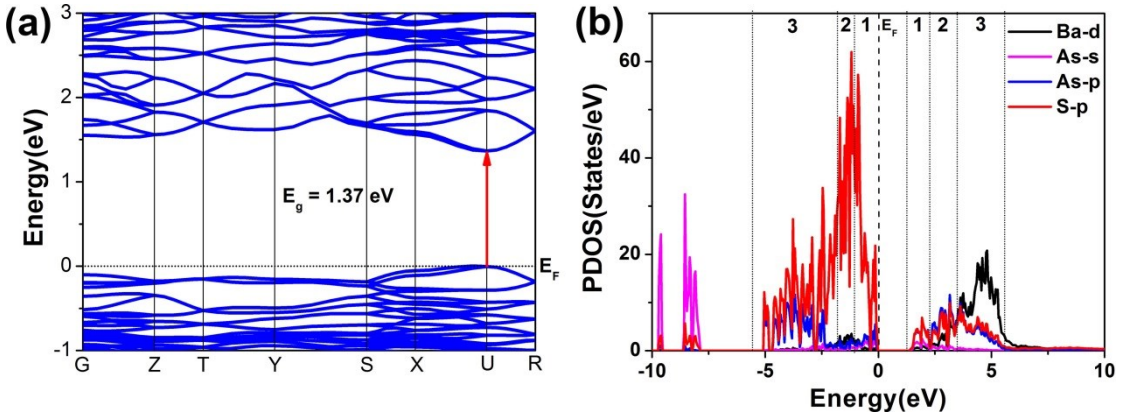

Figure S8. Theoretical calculation results of $Ba_2As_2S_5$: (a) band structure; (b) PDOSs [only the states with major contributions are given and the Fermi level (E_F) is set at 0.0 eV].

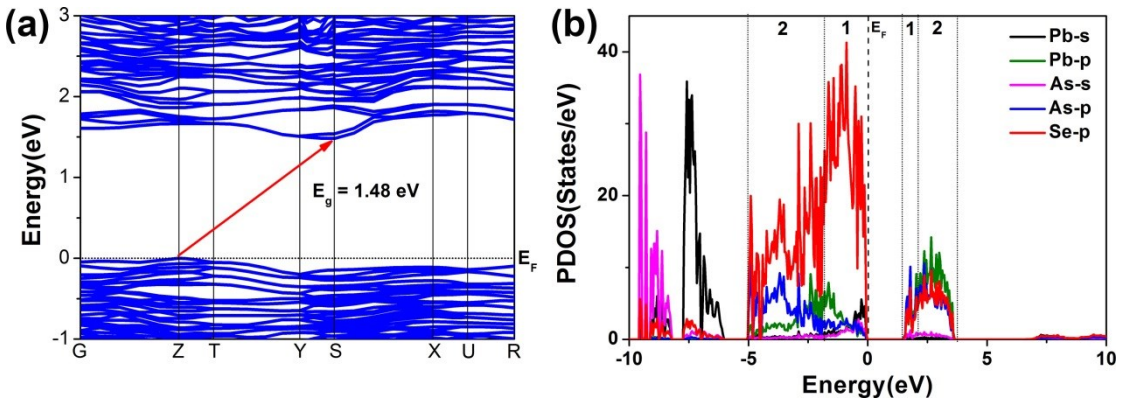

Figure S9. Theoretical calculation results of $Pb_2As_2S_5$: (a) band structure; (b) PDOSs [only the states with major contributions are given and the Fermi level (E_F) is set at 0.0 eV].

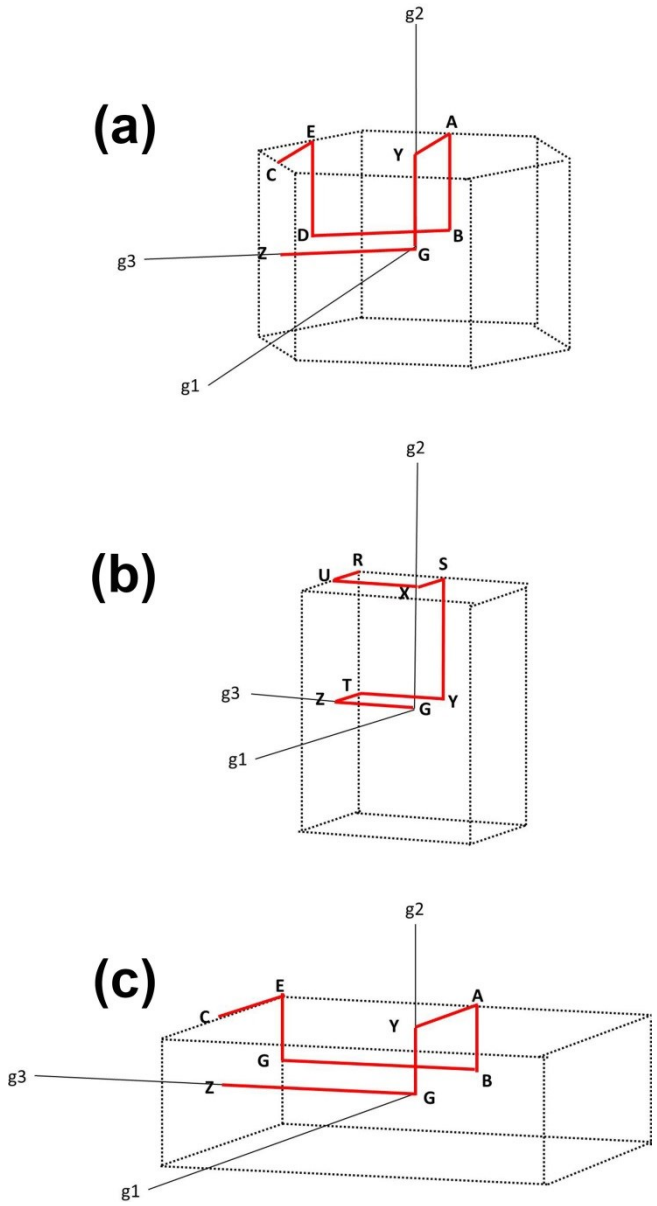

Figure S10. The first Brillouin zone with high symmetry points of (a) $Ba_2As_2Se_5$, (b) $Ba_2As_2S_5$ and (c) $Pb_2As_2S_5$.

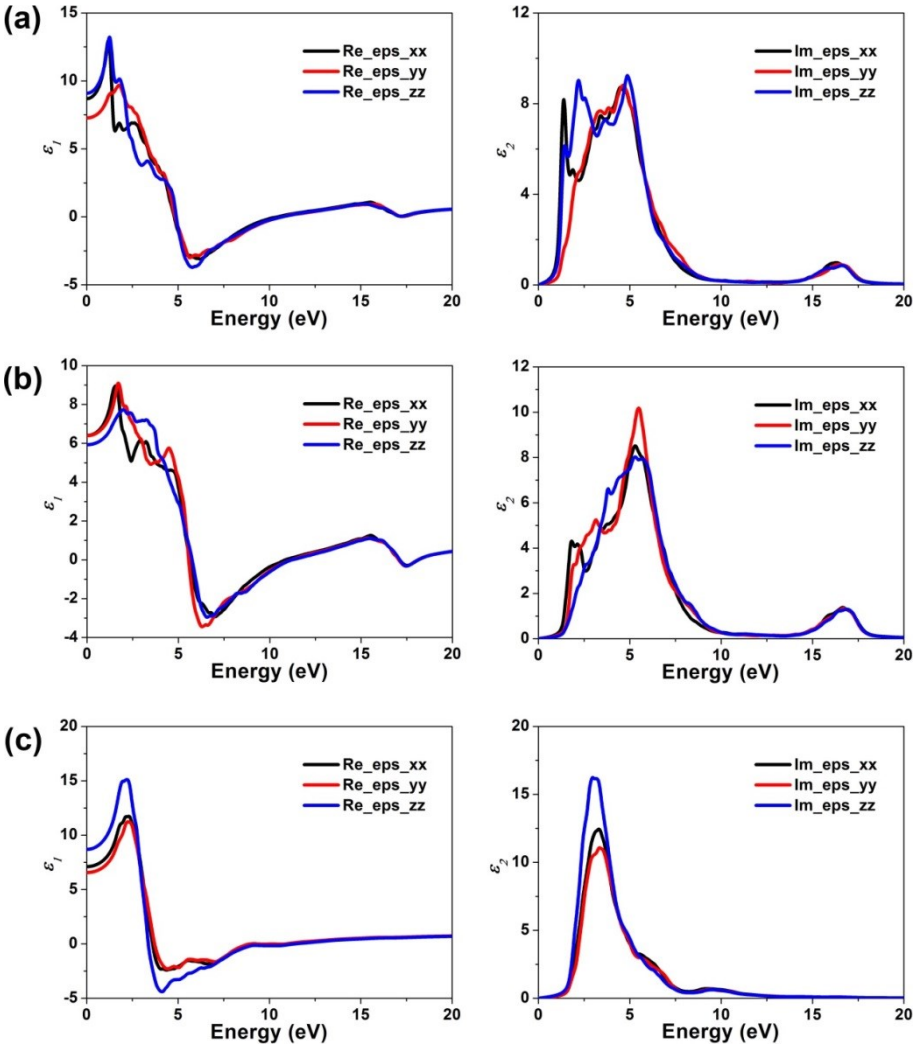

Figure S11. Energy dependences of the real part (ε_1) and imaginary part (ε_2) of (a) $Ba_2As_2Se_5$, (b) $Ba_2As_2S_5$ and (c) $Pb_2As_2S_5$.

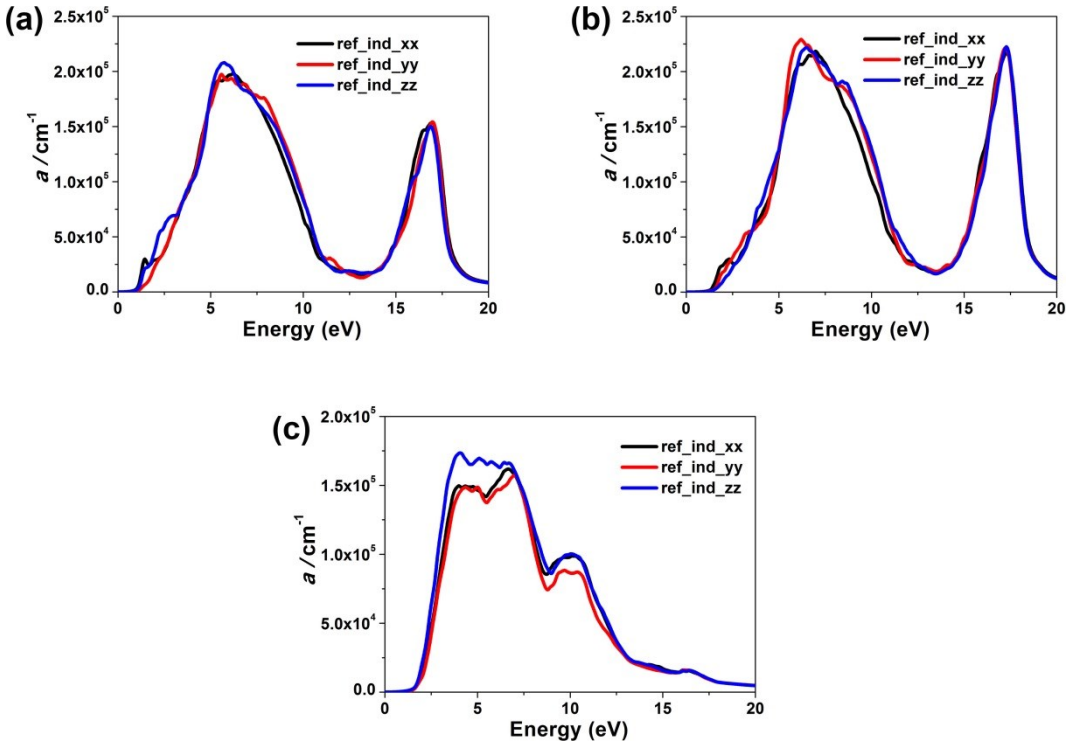

Figure S12. The calculated absorption coefficient (α) of (a) $Ba_2As_2Se_5$, (b) $Ba_2As_2S_5$ and (c) $Pb_2As_2S_5$.

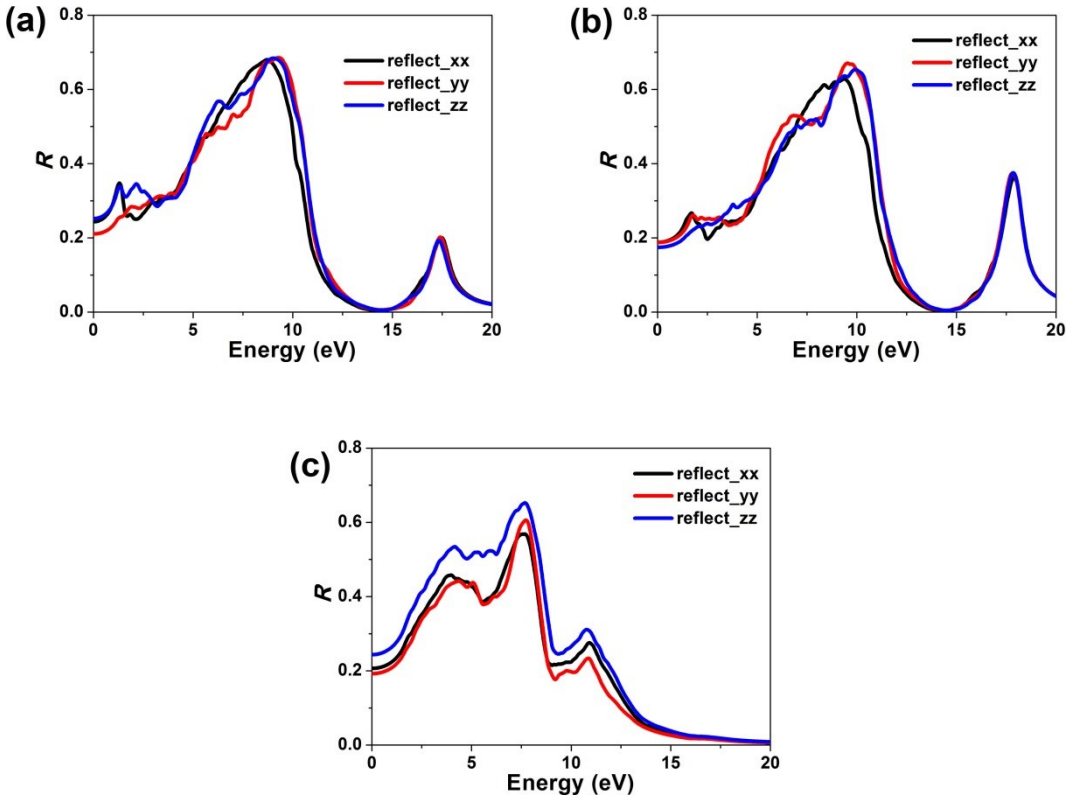

Figure S13. The calculated reflectivity (R) of (a) $Ba_2As_2Se_5$, (b) $Ba_2As_2S_5$ and (c) $Pb_2As_2S_5$.

Table S1 The lattice energy (LE) and lattice energy density (LED).

Compounds	LE/[Kcal/mol]	Volume of unit cell/[Å^3]	LED[a]/[Kcal/(mol*Å^3)]
$Ba_2As_2Se_5$	139779	1051.57	132.92
$Ba_2As_2S_5$	294673	1917.87	153.65
$Pb_2As_2S_5$	611933	1701.97	359.54
$AgGaS_2$	8488	341.52	24.85

[a]LED = LE/(volume of unit cell).

Table S2 The electronic states or arsenate(III) anions with major contributions in the VBs and CBs for $Ba_2As_2Se_5$.

	VB-1	**CB-1**
As-s	0.67%	0.89%
As-p	2.09%	6.22%
Se-p	26.17%	12.80%
[As(1)Se$_3$]	**28.92%**	**19.91%**
As-s	0.65%	0.93%
As-p	2.12%	6.07%
Se-p	25.88%	12.70%
[As(4)Se$_3$]	**28.65%**	**19.71%**
As-s	1.77%	1.05%
As-p	3.33%	15.99%
Se-p	30.88%	19.66%
[As$_2$Se$_4$]	**35.98%**	**36.70%**
Ba-d	6.45%	23.69%
Ba	**6.45%**	**23.69%**

Table S3 The electronic states or arsenate(III) anions with major contributions in the VBs and CBs for $Ba_2As_2S_5$.

	VB-3	**VB-1**	**CB-1**	**CB-3**
As-s	0.31%	1.18%	4.91%	0.26%
As-p	7.06%	2.95%	2.81%	4.90%
S-p	19.57%	22.35%	16.30%	9.34%
[As(3)S_3]	**26.95%**	**26.48%**	**24.02%**	**14.50%**
As-s	0.32%	1.24%	4.42%	0.29%
As-p	7.14%	3.06%	2.41%	4.29%
S-p	20.96%	25.40%	16.09%	9.50%
[As(4)S_3]	**28.42%**	**29.70%**	**22.92%**	**14.08%**
As-s	0.97%	3.17%	2.89%	0.45%
As-p	13.76%	4.25%	26.80%	8.18%
S-p	27.96%	32.37%	18.28%	10.58%
[As_2S_4]	**42.69%**	**39.79%**	**47.98%**	**19.21%**
Ba-d	1.94%	4.03%	5.09%	52.21%
Ba	**1.94%**	**4.03%**	**5.09%**	**52.21%**

Table S4 The electronic states or arsenate(III) anions with major contributions in the VBs and CBs for $Pb_2As_2S_5$.

	VB-1	**CB-1**
S-p	5.40%	1.11%
[S^{2-}]	**5.40%**	**1.11%**
As-s	0.65%	0.19%
As-p	0.92%	2.94%
S-p	9.52%	6.71%
[AsS_3]	**11.09%**	**9.83%**
As-s	1.39%	1.65%
As-p	2.71%	11.29%
S-p	23.75%	12.68%
[As_3S_7]	**27.85%**	**25.62%**
As-s	2.10%	1.68%
As-p	3.65%	13.37%
S-p	30.87%	20.08%
[As_4S_9]	**36.62%**	**35.13%**
Pb-s	7.21%	0.91%
Pb-p	11.82%	27.39%
Pb	**19.03%**	**28.30%**

4. References

1. P. Kubelka, *Z. Tech. Phys.*, 1931, **12**, 593–601.

2. S. K. Kurtz and T. T. Perry, *J. Appl. Phys.*, 1968, **39**, 3798–3813.

3. M. J. Zhang, X. M. Jiang, L. J. Zhou and G. C. Guo, *J. Mater. Chem. C*, 2013, **1**, 4754–4760.

4. G. Kresse, VASP, 5.3.5; http://cms.mpi.univie.ac.at/vasp/vasp/vasp.html, 2014.

5. G. Kresse, J. Furthmuller, *Phys. Rev. B: Condens. Matter*, 1996, 11169–11186.

6. G. Kresse and D. Joubert, *Phys. Rev. B: Condens. Matter*, 1999, **59**, 1758–1775.

7. P. E. Blochl, *Phys. Rev. B: Condens. Matter*, 1994, **50**, 17953–17979.

8. J. P. Perdew, K. Burke and M. Ernzerhof, *Phys. Rev. Lett.*, 1996, **77**, 3865–3868.

9. D. J. Chadi, *Phys. Rev. B: Condens. Matter*, 1976, **16**, 1746–1747.

10. C. Aversa and J. E. Sipe, *Phys. Rev. B*, 1995, **52**, 14636–14645.

11. S. N. Rashkeev, W. R. L. Lambrecht and B. Segall, *Phys. Rev. B*, 1998, **57**, 3905–3919.